



# Characterisation of Medipix3 Silicon Detectors in a Charged-Particle Beam

K. Akiba<sup>1</sup>, J. Alozy<sup>2</sup>, R. Aoude<sup>3</sup>, M. van Beuzekom<sup>4</sup>, J. Buytaert<sup>2</sup>, P. Collins<sup>2</sup>,  
A. Dosil Suárez<sup>5</sup>, R. Dumps<sup>2</sup>, A. Gallas<sup>5</sup>, C. Hombach<sup>6</sup>, D. Hynds<sup>7</sup>, M. John<sup>8</sup>, A. Leflat<sup>9</sup>,  
Y. Li<sup>10</sup>, E. Pérez Trigo<sup>5</sup>, R. Plackett<sup>11</sup>, M. M. Reid<sup>12</sup>, P. Rodríguez Pérez<sup>6</sup>, H. Schindler<sup>2†</sup>,  
P. Tsopelas<sup>4</sup>, C. Vázquez Sierra<sup>5‡</sup>, J. J. Velthuis<sup>13</sup>, M. Wysokiński<sup>14</sup>

<sup>1</sup> *Universidade Federal do Rio de Janeiro, Rio de Janeiro, Brazil*

<sup>2</sup> *European Organization for Nuclear Research (CERN), Geneva, Switzerland*

<sup>3</sup> *Pontifícia Universidade Católica do Rio de Janeiro, Rio de Janeiro, Brazil*

<sup>4</sup> *Nikhef National Institute for Subatomic Physics, Amsterdam, The Netherlands*

<sup>5</sup> *Universidade de Santiago de Compostela, Santiago de Compostela, Spain*

<sup>6</sup> *School of Physics and Astronomy, University of Manchester, Manchester, United Kingdom*

<sup>7</sup> *School of Physics and Astronomy, University of Glasgow, Glasgow, United Kingdom*

<sup>8</sup> *Department of Physics, University of Oxford, Oxford, United Kingdom*

<sup>9</sup> *Institute of Nuclear Physics, Moscow State University (SINP MSU), Moscow, Russia*

<sup>10</sup> *Center for High Energy Physics, Tsinghua University, Beijing, China*

<sup>11</sup> *Diamond Light Source Ltd., Didcot, United Kingdom*

<sup>12</sup> *Department of Physics, University of Warwick, Coventry, United Kingdom*

<sup>13</sup> *H.H. Wills Physics Laboratory, University of Bristol, Bristol, United Kingdom*

<sup>14</sup> *AGH - University of Science and Technology, Faculty of Computer Science, Electronics and Telecommunications, Kraków, Poland*

## Abstract

While designed primarily for X-ray imaging applications, the Medipix3 ASIC can also be used for charged-particle tracking. In this work, results from a beam test at the CERN SPS with irradiated and non-irradiated sensors are presented and shown to be in agreement with simulation, demonstrating the suitability of the Medipix3 ASIC as a tool for characterising pixel sensors.

Published in JINST

© CERN on behalf of the LHCb collaboration, licence CC-BY-4.0.

<sup>†</sup>Corresponding author.

<sup>‡</sup>Corresponding author.



# 1 Introduction

As part of the upgrade of the LHCb experiment, scheduled for the second long shutdown of the LHC in 2018/19, the present microstrip-based Vertex Locator (VELO) is foreseen to be replaced by a silicon hybrid pixel detector [1] with an ASIC dubbed “VeloPix” which will be derived from the Medipix family of ASICs. Like its predecessors Medipix2, Timepix, Medipix3, and Timepix3, the VeloPix chip will feature a matrix of  $256 \times 256$  square pixels with a pitch of  $55 \mu\text{m}$ . Prior to the arrival of the Timepix3 ASIC, Timepix and Medipix3 were the most suitable devices for the qualification of prototype sensors for the VELO upgrade. Until the end of lifetime of the upgraded experiment, the pixels closest to the beam line ( $r = 5.1 \text{ mm}$ ) accumulate a fluence of up to  $8 \times 10^{15} \text{ 1 MeV n}_{\text{eq}} \text{ cm}^{-2}$ . Qualifying silicon sensors in terms of radiation hardness is therefore a key element of the VELO upgrade R&D programme.

Timepix silicon detectors have been characterised extensively in terms of charged-particle tracking performance [2]. Since the ASIC has per-pixel information on the collected charge in terms of a time-over-threshold (ToT) value, a direct measurement of the charge deposition spectrum is possible.

Medipix3 [3, 4] on the other hand is a pure counting chip which was designed primarily for photon imaging applications. In order to measure the deposited charge in the sensor one therefore has to resort to indirect methods (Section 3). Among the large-scale ASICs in the high-energy physics community, Medipix3 has been the first to be based on IBM 130 nm CMOS technology. Compared to the Timepix (which was fabricated in 250 nm technology), it is expected to be more radiation tolerant [5] and thus lends itself for testing irradiated sensors.

In this work, we report on measurements with irradiated and non-irradiated Medipix3 assemblies carried out in 2012 at the H8 beamline of the CERN North Area facility, using positively charged hadrons with a momentum of  $180 \text{ GeV}/c$ . These measurements are intended to provide a validation of the chip functionality and performance complementary to characterisation measurements using photon sources. In addition, they also represent a first step towards a comprehensive evaluation of the radiation hardness of silicon pixel sensors with the “Medipix footprint” of  $55 \times 55 \mu\text{m}^2$  pixels.

## 2 Setup

The Timepix telescope, described in Ref. [6], was used for reconstructing the tracks of particles crossing the Medipix3 device under test (DUT). In order to minimise the pointing error, the DUT was placed in the centre of the telescope. For reading out the Medipix3 chip, the “Merlin” data acquisition system [7] developed at the Diamond Light Source facility was used. The synchronisation of Timepix and Medipix3 is straightforward, as both ASICs work in a “camera-style” frame-based readout mode. An external circuit implemented using NIM modules was used for sending shutter opening and closing signals to the telescope and the device under test. The coincident firing of two scintillators located upstream and downstream of the telescope was used for counting the number of beam

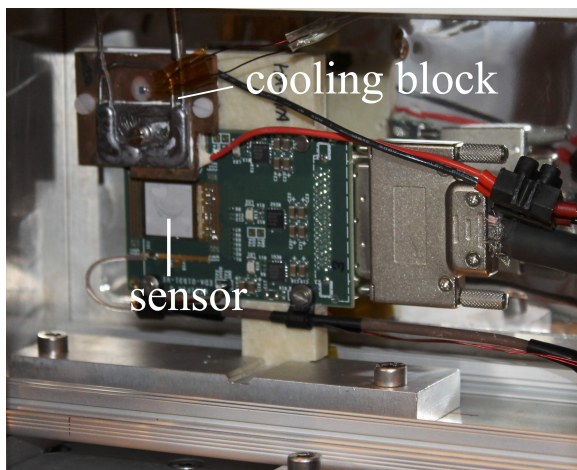


Figure 1: DUT mount and cooling setup. A Peltier cooler (not visible in the photograph) is clamped between the cooling block and the TPG sheet onto which the chip is glued.

particles traversing the telescope and the duration of a shutter was adjusted such that 50 scintillator triggers were accumulated in one frame. During one spill (9.6s) typically about 500 frames were recorded.

The temperature of the irradiated samples was controlled using a combination of thermoelectric and CO<sub>2</sub> cooling, the latter being provided by a portable cooling plant [8]. As can be seen on the photograph in figure 1, the chip was glued onto a tape of Thermal Pyrolytic Graphite (TPG) the other end of which was attached to the cold side of a Peltier cooler. The hot side of the Peltier cooler was put in contact with an aluminium cooling block through which CO<sub>2</sub> was circulating. With the chip switched off, a temperature of approximately  $-20^{\circ}\text{C}$  was reached, rising to  $-15^{\circ}\text{C}$  with the chip in operation. The setup was placed in a light-tight aluminium case which was flushed with nitrogen. The non-irradiated assemblies were measured at room temperature.

In all measurements discussed below, the DUTs were *n-on-p* silicon sensors bump-bonded to Medipix3.1 ASICs. The ASICs were operated in single-pixel high-gain mode and only one threshold (DAC THL) was used. Before taking data, a threshold equalisation was performed using the front-end noise as reference. The equalisation procedure consists of optimising the DAC values of two global current sources (ThresholdN and DACpixel) and the threshold adjustment bits of each pixel, such that the THL value corresponding to the noise floor lies within a certain window for all pixels. For the non-irradiated assemblies a target window of  $5 < \text{THL} < 25$  was used.

Prior to the beam test, calibration measurements using testpulses were performed to determine the relation between THL DAC and injected charge. To verify the viability of the testpulse method, data were taken with a <sup>241</sup>Am source for the two non-irradiated assemblies discussed below, and – after applying the calibrations obtained from the testpulse scan – the signal peaks were found to match within 2% between the two assemblies. These measurements were however made with a different readout system [9] and equalisation

mask than used in the testbeam (at that time the testpulse functionality was not yet implemented in Merlin).

Where possible<sup>1</sup>, calibration measurements using test pulses were later (after the beam test) made also using the Merlin system. These calibration curves are used in the following for a relative comparison of the signals measured with different sensors.

### 3 Measurements

For each track reconstructed in the telescope, the intercept with the DUT plane is calculated. In order to suppress fake tracks a requirement on the track quality is applied and the tracks are required to include hits on all telescope planes. If an unused cluster with a centre of gravity within a radius  $r_w = 110 \mu\text{m}$  around the track intercept is found, it is associated to the track and tagged as used. In case of multiple candidate clusters, the closest one is selected. The hit efficiency (or cluster finding efficiency)  $\varepsilon$  is then given by the fraction of tracks with an associated cluster on the DUT. The pointing resolution of the telescope ( $\sim 1.5 \mu\text{m}$  in the present configuration) allows one to probe the hit efficiency as function of the track intercept within a pixel cell. In the analysis we divide the pixel cell in  $9 \times 9$  bins and calculate separate efficiencies for each bin.

The most probable value (MPV) of the deposited charge can be estimated by scanning the hit efficiency as function of threshold. Assuming that the distribution of the collected charge can be described by a Landau distribution  $f_L$  convoluted with a Gaussian distribution  $f_G$ , the hit efficiency as a function of the threshold  $Q$  is given by

$$\varepsilon(Q) = \int_Q^\infty dx f_L \otimes f_G(x). \quad (1)$$

By fitting the measured efficiency with Eq. (1), the MPV and width of the Landau distribution and the  $\sigma$  of the Gaussian can be determined (the mean of the Gaussian is fixed to zero). This method requires that the entire charge deposited by a track is collected by a single pixel. We therefore use the hit efficiency in the central bin of the  $9 \times 9$  matrix for this measurement.

To determine the spatial resolution, the distributions of the residuals between the  $x, y$  coordinates of the track intercepts and the associated clusters are calculated. The standard deviation of the residual distribution is used as a resolution metric (the pointing error of the telescope represents only a small correction when subtracted in quadrature).

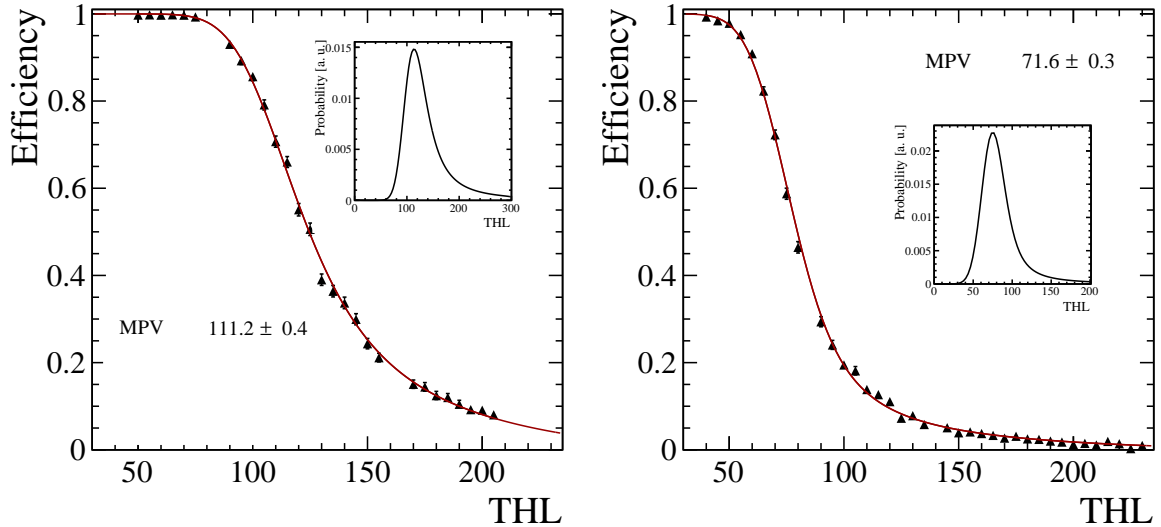


Figure 2: Hit efficiency (for tracks crossing the centre of a pixel cell) in non-irradiated Medipix3 assemblies with 100  $\mu\text{m}$  thick *n-on-p* sensors as function of threshold, for (left) assembly W20\_B6 and (right) assembly W20\_J9. The insets show the distribution of the charge deposition in units of THL. The error bars represent the statistical uncertainty of the measurements. For several points the error bars are smaller than the symbols.

## 4 Results

### 4.1 Non-irradiated assemblies

The measurements before irradiation were carried out using *n-on-p* active-edge sensors with a nominal thickness of 100  $\mu\text{m}$  manufactured by VTT<sup>2</sup>. The MPV of the charge deposition spectrum is thus expected to be around 7000 – 7500 electrons.

Two assemblies, W20\_B6 and W20\_J9, were tested with beam. After the beam test, part of the backside metallisation was removed from the sensor on W20\_B6, and by injecting laser pulses the depletion voltage  $V_{\text{dep}}$  was determined to be approximately  $-15\text{ V}$ . In the beam test, both sensors were operated at a bias voltage of  $-60\text{ V}$ , and were oriented perpendicularly to the beam. For each point in the threshold scan, a data set comprising typically  $1 - 2 \times 10^5$  reconstructed telescope tracks was recorded.

From the hit efficiency in the centre of the pixel cell as function of threshold (figure 2), the most probable value of the charge deposition spectrum is determined to correspond to  $\text{THL} \sim 111.2$  for assembly W20\_B6 and  $\text{THL} \sim 71.6$  for assembly W20\_J9. The statistical errors of the fit values are given in figure 2. Uncertainties due to tracking cuts, alignment, non-linearity of the THL DAC give rise to a systematic error on the MPV of  $\sim \pm 2.5\%$ . The MPVs in terms of THL DAC values differ significantly between the two devices. This

<sup>1</sup>One of the assemblies (W20\_B6) was accidentally damaged after the beam test.

<sup>2</sup>VTT Technical Research Centre of Finland, Espoo, Finland

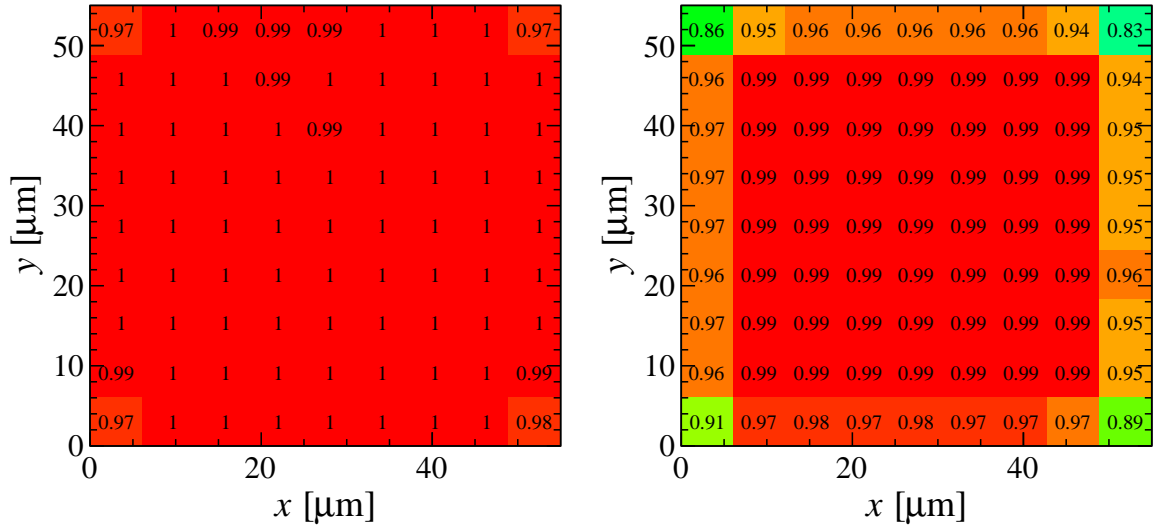


Figure 3: Hit efficiency in non-irradiated Medipix3 assemblies with 100  $\mu\text{m}$  thick sensors as function of the track intercept within a pixel cell, for (left) assembly W20\_B6 at  $\text{THL}/\text{MPV} \sim 0.45$  and (right) assembly W20\_J9 at  $\text{THL}/\text{MPV} \sim 0.56$ .

can be attributed to non-optimised settings of the DAC “Vcas” (for voltage cascode), which sets the reference voltage for some transistors in the pixel circuit and, if not tuned properly, can have an impact on the operating point of the circuit.

As discussed in section 2, testpulse calibration measurements using the Merlin readout system could only be made for assembly W20\_J9. To facilitate the comparison between the devices, the results discussed below are therefore presented as function of the threshold-to-signal ratio, i. e. the applied THL DAC normalised to the respective MPV.

Figure 3 (left) shows the hit efficiency as function of the track intercept within a pixel cell for the lowest threshold-to-signal ratio ( $\text{THL}/\text{MPV} \sim 0.45$ ) covered by the threshold scan. At this threshold – which is high compared to a typical operational threshold of 1000 electrons – the detector can be seen to be fully efficient ( $\varepsilon > 0.99$ ), except at the corners. With increasing threshold – as illustrated in figure 3 (right) – a drop in efficiency becomes noticeable at the borders of the pixel cell. This is a consequence of charge sharing due to diffusion, as can be seen from figure 4 which shows the average cluster size as function of the track intercept within the pixel cell.

Figure 5 (left) shows the average cluster size as function  $\text{THL}/\text{MPV}$ . At the lowest threshold, an average cluster size of  $1.103 \pm 0.001$  is found, with single-pixel clusters constituting  $\sim 91.3\%$  and two-pixel clusters  $\sim 7.7\%$  of all associated clusters. The cluster size as function of threshold/signal follows the same shape for both sensors, exhibiting a minimum around  $\text{THL}/\text{MPV} \sim 0.9$  and a subsequent maximum around  $\text{THL}/\text{MPV} \sim 1.6$ . With increasing threshold, an increasing fraction of the observed clusters is produced by primary particles which suffer collisions with large energy loss. These collisions give rise to energetic electrons which further ionise along their path and produce electron-hole pairs

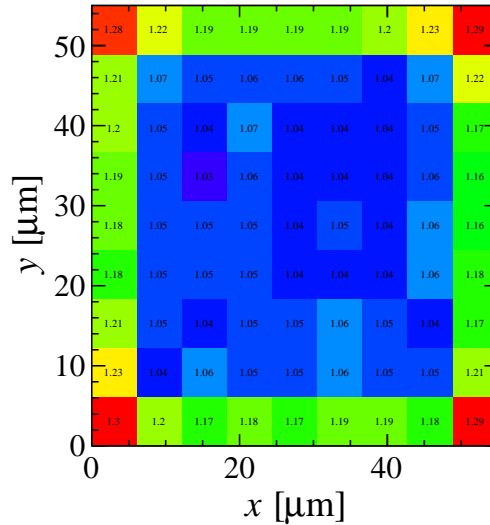


Figure 4: Average cluster size as function of the track intercept within a pixel cell for assembly W20\_B6 (100  $\mu\text{m}$  thick sensor) at  $\text{THL}/\text{MPV} \sim 0.45$ . Multi-pixel clusters are found predominantly at the edges and corners of the pixel cell.

away from the trajectory of the primary particle.

The residual distributions (in the  $x$  direction) at low threshold for one-pixel and two-pixel clusters are shown in figure 6. Averaged over all cluster sizes, the standard deviation of the residual distribution is found to be  $\sim 15.7 \mu\text{m}$  in both  $x$  and  $y$ . As expected from the dominance of one-pixel clusters, this value is close to the binary limit ( $55 \mu\text{m}/\sqrt{12} \sim 15.9 \mu\text{m}$ ). Figure 5 (right) shows the  $\sigma$  of the residual distribution in  $x$  as function of threshold/signal. The resolution can be seen to deteriorate significantly after the threshold crosses the MPV.

Figure 5 also includes results obtained with a Timepix ASIC bump-bonded to a 100  $\mu\text{m}$  thick  $n$ -on- $p$  sensor from the same batch. The Timepix assembly was measured in the same beam test campaign and was operated at a threshold of 1000 electrons and a bias voltage of  $-60 \text{ V}$ . The data were taken in ToT mode, but the values shown in figure 5 were calculated with the ToT values set to one to mimic the Medipix3 behaviour. The results for the Timepix assembly are in agreement with the extrapolated results from the Medipix3 assemblies.

To understand better the observed shapes of resolution and cluster size as function of threshold, a simple simulation using the Garfield++ toolkit [10] was used. The primary ionisation process is calculated using the Heed program [11], which in addition to the energy loss by the traversing charged particle also simulates the ionisation cascade from high-energy (“delta”) electrons produced in the interactions of the charged particle with the silicon medium as well as the spatial distribution of the resulting electron-hole pairs. Each electron is subsequently transported through the sensor, based on the drift velocity and diffusion coefficient as function of the electric field. A one-dimensional approximation

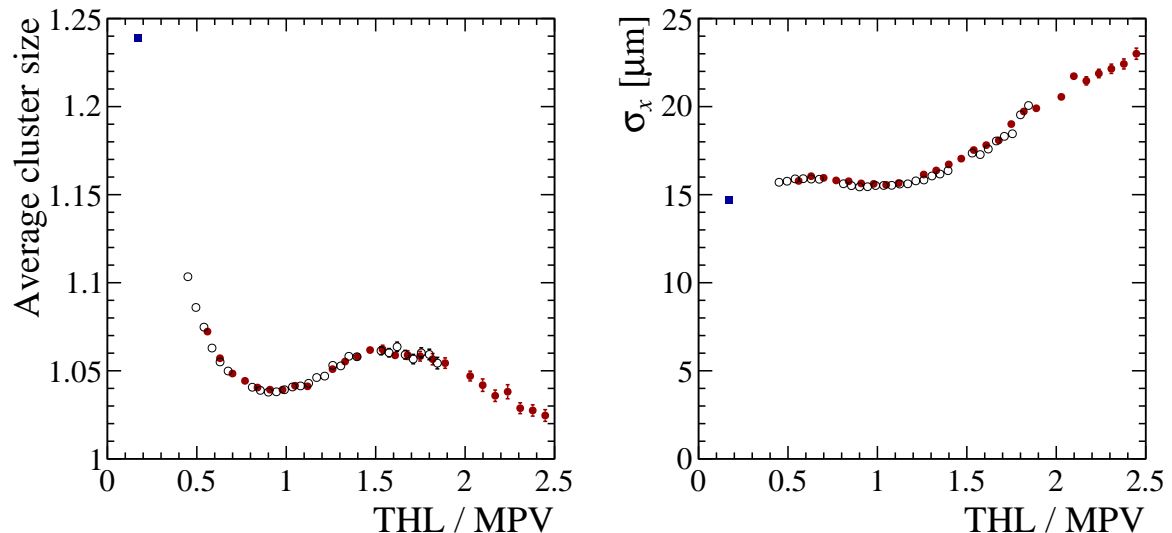


Figure 5: Average cluster size (left) and standard deviation of the  $x$ -residual distribution (right) at perpendicular track incidence as function of threshold-to-signal ratio for assemblies W20\_B6 (empty circles) and W20\_J9 (full circles). Results for a Timepix assembly with the same type of sensor are shown with full squares. The error bars represent the statistical uncertainty of the measurements. For most points the error bars are smaller than the symbols.

for the electric field is used<sup>3</sup>.

As can be seen from figure 7, the features in the measured cluster size and resolution as function of threshold-to-signal ratio are reproduced by the simulation, provided that the spatial extent of the ionisation pattern is taken into account. This corroborates the conclusion that these features are due to “delta” electrons.

## 4.2 Irradiated assemblies

A set of Medipix3.1 assemblies, with VTT  $n$ -on- $p$  active-edge sensors from the same batch as the non-irradiated sensors discussed above, were irradiated at the Ljubljana TRIGA reactor [12] to a 1 MeV neutron equivalent fluence of  $5 \times 10^{14} \text{ cm}^{-2}$  and subsequently annealed for 80 minutes at  $60^\circ \text{ C}$ . From lab measurements with a laser, the effective depletion voltage  $V_{\text{dep}}$  of these sensors after irradiation was measured to be between  $-85$  and  $-105 \text{ V}$ . One of the assemblies, W20\_H5, was characterised in the beam test. The sensor, which has a pixel-to-edge distance of  $100 \text{ }\mu\text{m}$ , was operated at a bias voltage of  $-100 \text{ V}$  as operation at higher bias was inhibited by the onset of electrical breakdown (figure 8).

In general, the irradiated assemblies exhibited a higher dark count rate compared to the non-irradiated ones, which was attributed to electrons from the  $\beta$ -decay of  $^{182}\text{Ta}$

<sup>3</sup>The electric field is assumed to vary linearly between  $E = (V - V_{\text{dep}})/d$  at the sensor backside and  $E = (V + V_{\text{dep}})/d$  at the implants, where  $d$  is the sensor thickness.

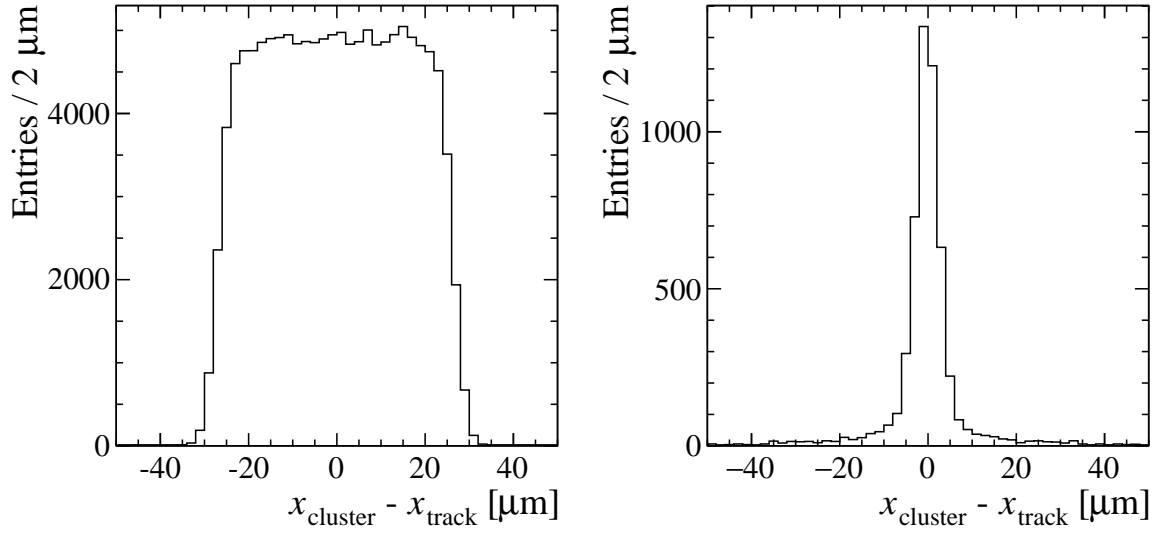


Figure 6: Residual distribution for (left) one-pixel and (right) two-pixel clusters extending over two columns in a non-irradiated 100  $\mu\text{m}$  thick sensor (assembly W20\_B6, at  $\text{THL}/\text{MPV} \sim 0.45$ ).

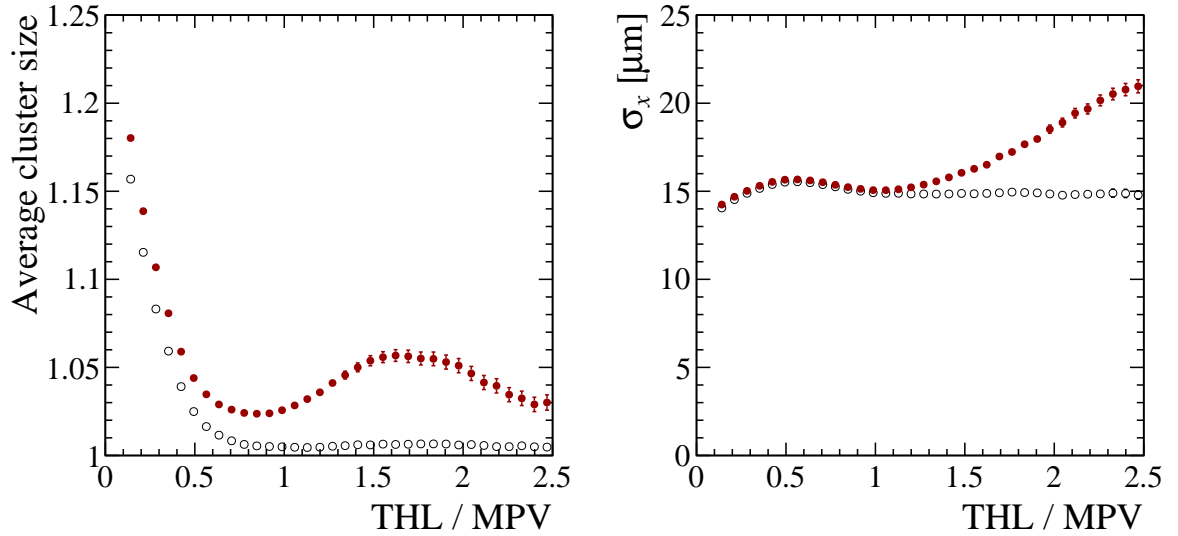


Figure 7: Simulated average cluster size (left) and standard deviation of the  $x$ -residual distribution (right) at perpendicular track incidence as function of threshold-to-signal ratio. Full (empty) symbols show the results with (without) the spatial extent of the ionisation pattern being included in the simulation.

produced by neutron activation during the irradiation of the ASIC<sup>4</sup>. This – presumably in combination with other radiation effects – resulted in problems during the equalisation

<sup>4</sup> The presence of  $^{182}\text{Ta}$  in the irradiated assemblies was confirmed by gamma spectroscopy measurements performed by the CERN radioprotection group.

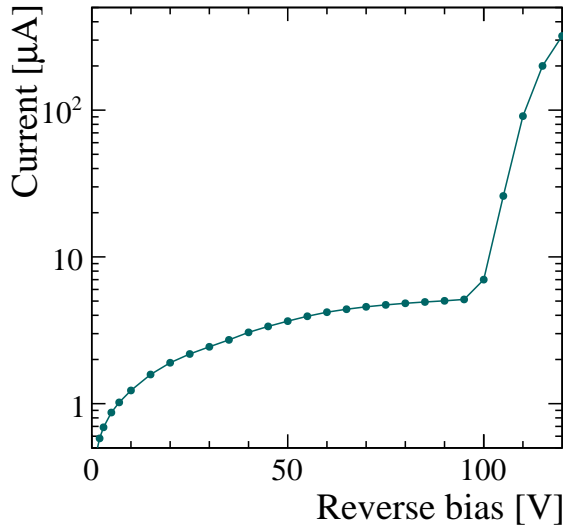


Figure 8: Leakage current as function of reverse bias voltage at  $T = -13^\circ\text{C}$  after irradiation to  $0.5 \times 10^{15} \text{ 1 MeV n}_{\text{eq}} \text{ cm}^{-2}$  (100  $\mu\text{m}$  thick  $n$ -on- $p$  active-edge sensor with 100  $\mu\text{m}$  pixel-to-edge distance).

procedure for some assemblies, as well as a larger threshold dispersion. The optimised values of the DACs which control the global currents (ThresholdN and DACpixel) were larger (by a factor 2 – 3) compared to the non-irradiated assemblies.

As can be seen from figure 9, the MPV of the charge deposition spectrum corresponds to a THL DAC of  $\sim 53.9$ . After correcting for the differences in gain and offset using testpulse calibration curves, this value is found to be approximately 8.5% lower than the MPV of the non-irradiated sensors.

As in the non-irradiated case, the cluster size spectrum is dominated by single-pixel clusters. Cluster size and  $\sigma$  of the  $x$ -residual distribution as function of threshold-to-signal ratio (figure 10) follow closely the corresponding curves for the non-irradiated assemblies (figure 5).

Figure 11 shows the hit efficiency as function of the track intercept within a pixel cell at the lowest measured threshold (THL = 40). In the centre of the pixel cell, an efficiency of  $0.93 \pm 0.01$  is found, compared to  $0.97 \pm 0.01$  for the non-irradiated assemblies at the same threshold-to-signal ratio ( $\sim 0.74$ ).

A further beam test measurement was performed with a Medipix3.1 ASIC bump-bonded to a 200  $\mu\text{m}$  thick  $n$ -on- $p$  sensor manufactured by CNM<sup>5</sup>. The sensor featured two guard rings and was diced at a distance of 400  $\mu\text{m}$  from the border of the pixel matrix. The assembly (W20\_D6) was also irradiated at Ljubljana, but to a higher fluence,  $2.5 \times 10^{15} \text{ 1 MeV n}_{\text{eq}} \text{ cm}^{-2}$ . During the equalisation procedure, a large threshold dispersion was observed, such that the upper limit of the equalisation target window needed to be increased to THL = 40. In addition, a significant fraction ( $\sim 10\%$ ) of the pixels needed

<sup>5</sup>Centro Nacional de Microelectrónica, Barcelona, Spain

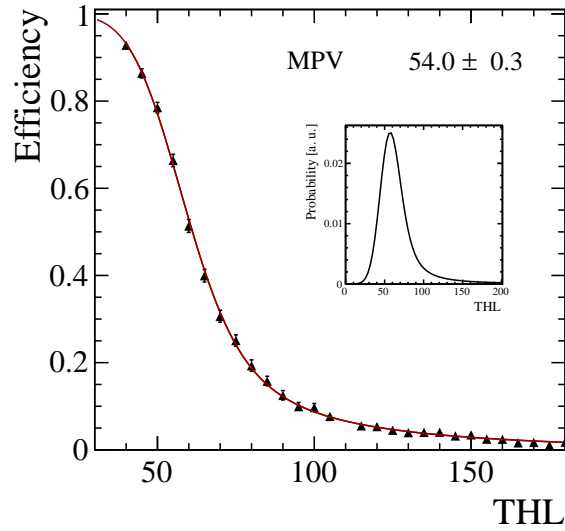


Figure 9: Hit efficiency in Medipix3 assembly W20\_H5 with 100  $\mu\text{m}$  thick *n-on-p* sensor as function of threshold, after irradiation to  $0.5 \times 10^{15}$   $1 \text{ MeV n}_{\text{eq}} \text{ cm}^{-2}$ . The inset shows the distribution of the charge deposition in units of THL (Landau distribution convoluted with a Gaussian).

to be masked. Tracks crossing a masked pixel were thus excluded from the efficiency measurements for this device.

Because of time constraints, data were taken only at three THL values with this device, such that determining the MPV of the charge deposit spectrum was not possible.

Figure 12 shows the efficiency as function of the track intercept. The dependency of the efficiency on the applied threshold and bias voltage is shown in figure 13.

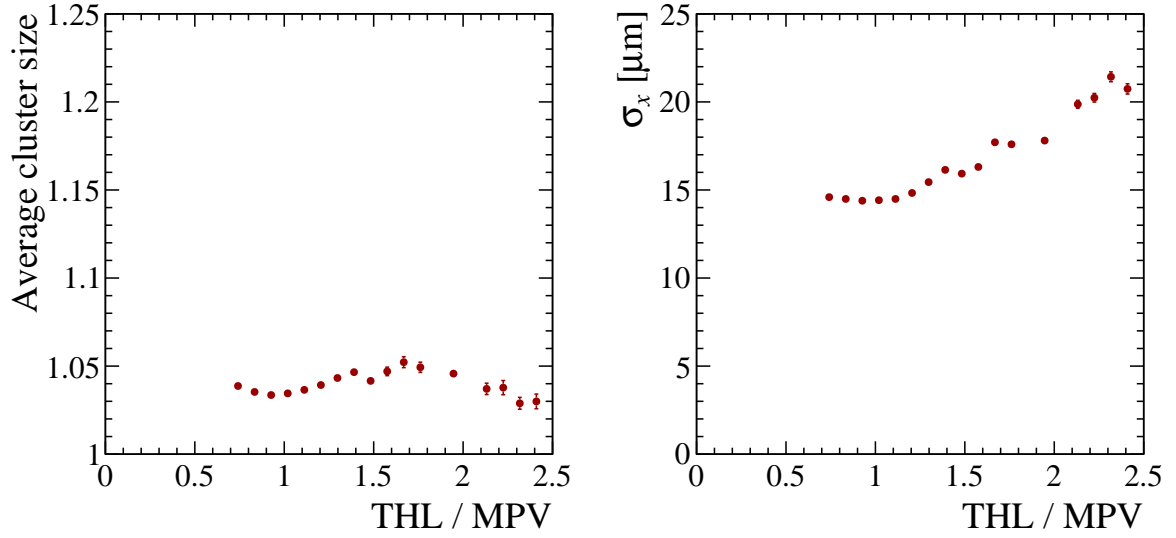


Figure 10: Average cluster size (left) and standard deviation of the  $x$ -residual distribution (right) at perpendicular track incidence as function of threshold-to-signal ratio for irradiated assembly W20\_H5.

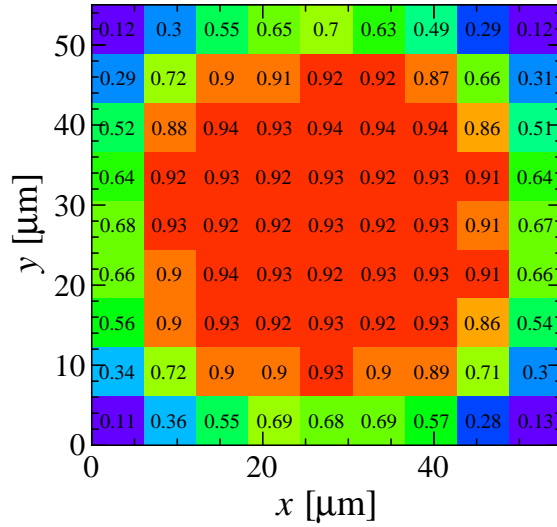


Figure 11: Hit efficiency in Medipix3 assembly W20\_H5 with 100 μm thick  $n$ -on- $p$  sensor as function of the track intercept within a pixel cell at THL = 40 (threshold/signal  $\sim 0.74$ ), after irradiation to  $0.5 \times 10^{15}$  1 MeV  $n_{\text{eq}}$   $\text{cm}^{-2}$ . The drop in efficiency at the edges of the pixel cell is more pronounced than in figure 3 mainly because of the higher threshold-to-signal ratio.

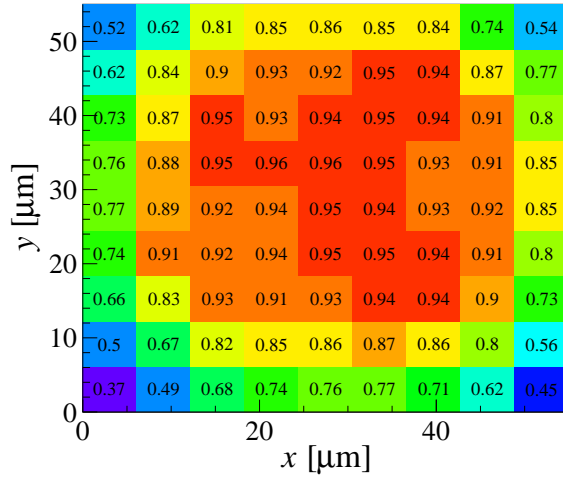


Figure 12: Hit efficiency in Medipix3 assembly W20\_D6 with 200  $\mu\text{m}$  thick *n-on-p* sensor (diced at 400  $\mu\text{m}$  from the last pixel) as function of the track intercept within a pixel cell at  $\text{THL} = 50$  and 300 V bias voltage, after irradiation to  $2.5 \times 10^{15} \text{ 1 MeV n}_{\text{eq}} \text{ cm}^{-2}$ . The asymmetry of the efficiency profile is attributed to a small inclination of the assembly with respect to the beam.

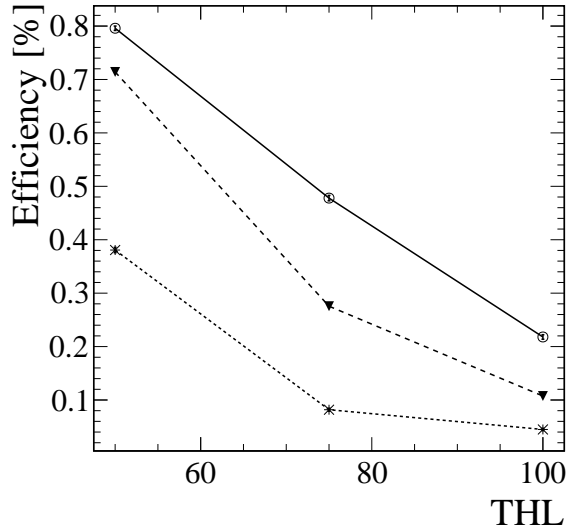


Figure 13: Overall hit efficiency in irradiated assembly W20\_D6 with 200  $\mu\text{m}$  thick *n-on-p* sensor as function of the THL value for different bias voltages (stars:  $-100 \text{ V}$ , triangles:  $-200 \text{ V}$ , circles:  $-300 \text{ V}$ ). The assembly was irradiated to a fluence of  $2.5 \times 10^{15} \text{ 1 MeV n}_{\text{eq}} \text{ cm}^{-2}$ . The lines are drawn to guide the eye.

## 5 Conclusions

First results on the performance of hadron-irradiated pixel detectors with the “footprint” of the upgraded LHCb VELO ( $55 \times 55 \mu\text{m}^2$  pixels) have been obtained from a beam test at the CERN SPS, using Medipix3.1 ASICs bump-bonded to thin *n-on-p* silicon sensors. As the Medipix3 ASICs do not provide a direct measurement of the collected charge, threshold scans were used for characterising the sensor.

Reference measurements with non-irradiated Medipix3.1 assemblies were made in the same testbeam campaign. The threshold DAC value (THL) corresponding to the most probable value of the charge deposition spectrum was determined from the hit efficiency as function of threshold. The measured cluster size and resolution as function of the THL/MPV ratio are consistent between the assemblies and in good agreement with simulations.

After irradiation with reactor neutrons to a fluence of  $0.5 \times 10^{15} \text{ 1 MeV n}_{\text{eq}} \text{ cm}^{-2}$ , a larger threshold dispersion and an increased power consumption of the ASIC were observed. A direct comparison between the performance of irradiated and non-irradiated sensors is complicated due to the fact that the non-irradiated sensors were operated at overdepletion while the irradiated sensor (due to early electrical breakdown) needed to be operated close to depletion. The difference in operating conditions may explain the small drop in efficiency and MPV measured with the irradiated sensor. The shapes of average cluster size and resolution versus threshold are not changed significantly compared to the non-irradiated sensors.

The studies presented in this paper are being continued using the Timepix3 ASIC, which has recently become available.

## Acknowledgements

We gratefully acknowledge strong support from the CERN Medipix Group, in particular Rafael Ballabriga. We would also like to thank Juha Kalliopuska and Sami Vähänen from VTT/Advacam and Giuglio Pellegrini from the IMB-CNM Radiation Detectors Group. The research leading to these results has received partial funding from the European Commission under the FP7 Research Infrastructures project AIDA, grant agreement no. 262025. We gratefully acknowledge the expert wire bonding support provided by Ian McGill of the CERN DSF bonding lab. We extend warm thanks to Igor Mandić and Vladimir Cindro for irradiating the Medipix3 assemblies.

## References

- [1] LHCb collaboration, R. Aaij et al., *LHCb VELO Upgrade Technical Design Report*, CERN-LHCC-2013-021. LHCb-TDR-013.

- [2] K. Akiba et al., *Charged particle tracking with the Timepix ASIC*, *Nucl. Instr. Meth. A* **661** (2012), 31–49, [arXiv:1103.2739]
- [3] R. Ballabriga, M. Campbell, E. Heijne, X. Llopart, L. Tlustos, and W. Wong, *Medipix3: A 64 k pixel detector readout chip working in single photon counting mode with improved spectrometric performance*, *Nucl. Instr. Meth. A* **633** (2011), S15 – S18
- [4] R. Ballabriga et al., *Characterization of the Medipix3 pixel readout chip*, 2011 *JINST* **6** C01052
- [5] R. Plackett, X. Llopart, R. Ballabriga, M. Campbell, L. Tlustos, and W. Wong, *Measurement of Radiation Damage to 130 nm Hybrid Pixel Detector Readout Chips*, Proceedings of Topical Workshop on Electronics for Particle Physics (TWEPP09), CERN-2009-006
- [6] K. Akiba et al., *The Timepix Telescope for high performance particle tracking*, *Nucl. Instr. Meth. A* **723** (2013), 47–54, [arXiv:1304.5175]
- [7] R. Plackett, I. Horswell, E. N. Gimenez, J. Marchal, D. Omar, and N. Tartoni, *Merlin: a fast versatile readout system for Medipix3*, 2013 *JINST* **8** C01038
- [8] B. Verlaat, L. Zwalinski, R. Dumps, M. Ostrega, P. Petagna, and T. Szwarc, *TRACI, a multipurpose CO<sub>2</sub> cooling system for R&D*, 10<sup>th</sup> IIR-Gustav Lorentzen Conference on Natural Working Fluids (2012), Refrigeration Science and Technology Proceedings 2012-1
- [9] D. Tureček et al., *Pixelman: a multi-platform data acquisition and processing software package for Medipix2, Timepix and Medipix3 detectors*, 2011 *JINST* **6** C01046
- [10] *Garfield++ – simulation of tracking detectors*, <http://cern.ch/garfieldpp>
- [11] I. B. Smirnov, *Modeling of ionization produced by fast charged particles in gases*, *Nucl. Instr. Meth. A* **554** (2005), 474 – 493
- [12] L. Snoj, G. Žerovnik, A. Trkov, *Computational analysis of irradiation facilities at the JSI TRIGA reactor*, *Applied Radiation and Isotopes* **70** (2012), 483–488